JOURNAL OF SYNCHROTRON RADIATION

ISSN 1600-5775

Received 18 September 2018
Accepted 20 May 2019

Edited by A. F. Craievich, University of São Paulo, Brazil

Keywords: X-ray diffraction; pulsed heating; elasticity; plasticity.

Dynamic observation of X-ray Laue diffraction on single-crystal tungsten during pulsed heat load

Aleksey S. Arakcheev,[a,b,c]* Vladimir M. Aulchenko,[a] Ilya I. Balash,[a,b,d] Aleksandr V. Burdakov,[a,c] Aleksandr D. Chernyakin,[a] Valentin A. Dokutovich,[a] Oleg V. Evdokov,[d] Aleksandr A. Kasatov,[a] Sergey R. Kazantsev,[a,b,d] Aleksandr V. Kosov,[a] Vladimir A. Popov,[a,b] Marat R. Sharafutdinov,[a,d] Lev I. Shekhtman,[a] Andrey A. Shoshin,[a,b] Boris P. Tolochko,[a,d] Aleksandr A. Vasilyev,[a] Leonid N. Vyacheslavov,[a,b] Liubov A. Vaigel[a,c] and Vladimir V. Zhulanov[a,b]

[a]Budker Institute of Nuclear Physics of Siberian Branch of the Russian Academy of Sciences, Novosibirsk, Russian Federation, [b]Novosibirsk State University, Novosibirsk, Russian Federation, [c]Novosibirsk State Technical University, Novosibirsk, Russian Federation, and [d]Institute of Solid State Chemistry and Mechanochemistry of Siberian Branch of the Russian Academy of Sciences, Novosibirsk, Russian Federation. *Correspondence e-mail: asarakcheev@gmail.com

The dynamics of the diffraction peak shape during pulsed heat load on mosaic single-crystal tungsten were measured at the 'Plasma' scattering station on the eighth beamline of the VEPP-4 synchrotron radiation source at the Budker Institute of Nuclear Physics. The observed evolution of the diffraction peak shape agrees with theoretical predictions based on calculations of deformation caused by pulsed heating. Three clearly distinguishable stages of the diffraction-peak evolution were found, correlating with the evolution of temperature and deformation distributions. The residual plastic deformation increased with subsequent heating pulses.

1. Introduction

The best results on heating and magnetic confinement of fusion plasma have been demonstrated at facilities based on a tokamak geometry of the magnetic field (Ongena *et al.*, 2016). The H-mode (a promising regime of plasma confinement in a tokamak) is accompanied by repetitive transient ejections of plasma on the divertor (Wagner, 2007). The pulsed behaviour of the plasma load on the divertor plates significantly intensifies the erosion of the material (De Temmerman *et al.*, 2018). Each pulse of the plasma load is a short intense flow of plasma particles to the material. In addition to more complex effects of the energetic particles, the plasma load leads to pulsed heating of the material. A sharp rise in the temperature of the thin surface layer is one cause of the intensification of erosion and mechanical destruction of the material. Cracking of the tungsten surface by pulsed heat loads has been observed experimentally (Linke *et al.*, 1992; Huber *et al.*, 2014; Loewenhoff *et al.*, 2015). Theoretical simulations demonstrate that the cracking is caused by plastic deformation occurring during heating and resulting in the formation of tensile stresses after cooling (Arakcheev, Huber *et al.*, 2015; Arakcheev, Skovorodin *et al.*, 2015). Note that several long-term heating–cooling cycles also result in cracking (so-called 'self-castellation'; Panayotis *et al.*, 2017) and the mechanism of tensile stress formation is similar to the case of pulsed heat load (Hirai *et al.*, 2016).

The difference between steady-state and pulsed heating appears in the thickness of the heated layer. In the case of

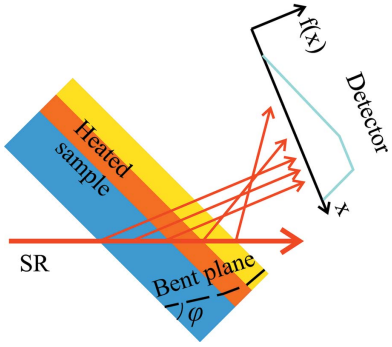

pulsed heating, the thin heated layer causes greater residual stresses for the same surface temperature rise. The stresses are localized in the heated-up surface layer due to the dependence of the plastic deformation on the local temperature rise only (Arakcheev *et al.*, 2015). Thus, the distributions of the stresses and deformations are localized near the surface and decrease rapidly with depth. The distributions determine the parameters of the cracking. Consequently, to study the cracking it is necessary to measure the depth distributions of the deformations and stresses. In addition, the measurements should be time-resolved during heating because the cracking parameters depend on the details of the temporal dependence of the load.

A suitable diagnostic based on the diffraction of synchrotron radiation has been proposed (Arakcheev *et al.*, 2016). The diagnostic does not require measurements at several different inclinations of the sample, as in the classical method of residual stress measurements in polycrystalline samples (Makhlaj *et al.*, 2009). The new diagnostic allows time-resolved measurements during pulsed processes. The main restriction of the diagnostic is that only a single crystal is used as a sample. The restriction is significant because usually real divertors are polycrystalline. However, at least the elastic properties of single-crystal tungsten are almost isotropic (Anderson & Brotzen, 1982), which means that the spatial distributions of stresses during elastic deformation under pulsed heating are similar in single-crystal and polycrystalline tungsten.

Our previous work demonstrated measurement of the dynamics of the change in the scattering angle (Arakcheev *et al.*, 2016), whereas calculation of the deformation distribution requires data on the change in the shape of the diffraction peak. This article presents the first results of the measurements of diffraction peak shape during pulsed heat load on a sample.

2. Experimental

2.1. X-ray diffraction

We use the method of measurement of material deformation based on X-ray diffraction in a single crystal. According to the laws of diffraction, the angle of incidence to a crystal plane is equal to the angle of reflection. Thus, a rotation of the atomic lattice plane because of deformation of the material leads to a change in the scattering angle. Note that the change in the scattering angle (and in the interplanar spacing) results in a change in the energy of the X-rays forming the diffraction peak according to the Bragg condition. Thus, it is necessary to use polychromatic synchrotron radiation to prevent disappearance of the diffraction peak during pulsed heating.

The deformation of a material caused by pulsed heat load is the result of differential thermal expansion. In the case of a short-pulsed heat load, the deformation is mostly displacements perpendicular to the exposed surface and the local relative strain is determined by the local temperature rise (Arakcheev, Huber *et al.*, 2015; Arakcheev, Skovorodin *et al.*, 2015). According to the solution of the linear elasticity problem, the elastic deformation is determined by the following expression:

$$\varepsilon_{zz} = \frac{1+\nu}{1-\nu}\,\alpha\,(T - T_0), \tag{1}$$

where ε_{ij} is the deformation tensor, z is the normal to the exposed surface coordinate, ν is Poisson's ratio, α is the linear coefficient of thermal expansion, T is the local temperature and T_0 is the initial (base) temperature. Other components of ε_{ij} equal zero.

Let us calculate the change in the angle φ between the crystal diffraction plane and the exposed surface, caused by the pulsed heat load. The tangent of the angle φ is the ratio of the cathetus perpendicular to the surface to the cathetus parallel to the surface. According to the known deformation, the specific elongation of the former is described by equation (1) and the length of the latter stays fixed. So, the tangent of the angle φ changes according to the following expression:

$$\tan(\varphi) = (1+\varepsilon_{zz})\tan(\varphi_0) = \left[1 + \frac{1+\nu}{1-\nu}\alpha(T - T_0)\right]\tan(\varphi_0), \tag{2}$$

where φ_0 is the initial value of φ before the pulsed heating. Assuming that the change in φ is small, we expand $\tan(\varphi)$ into a series to the first order:

$$\tan(\varphi_0) + \frac{1}{\cos^2(\varphi_0)}\,(\varphi - \varphi_0) = \left[1 + \frac{1+\nu}{1-\nu}\,\alpha\,(T - T_0)\right]\tan(\varphi_0). \tag{3}$$

After cancelling the zeroth order we obtain an expression for the change in the angle φ:

$$\varphi - \varphi_0 = \frac{1+\nu}{2(1-\nu)}\,\alpha\,(T - T_0)\sin(2\varphi_0). \tag{4}$$

While the local orientation of the crystal plane changes, the scattering angle of X-ray diffraction, 2θ, changes twofold:

$$\delta 2\theta = \frac{1+\nu}{1-\nu}\sin(2\varphi)\,\alpha\,(T - T_0). \tag{5}$$

Note that if the elastic deformation turns to plastic deformation, Poisson's ratio ν should be taken equal to 1/2. Expression (5) demonstrates the maximum change in the scattering angle at the same heating for $\varphi = 45^\circ$. It also shows that the change in scattering angle caused by elastic deformation is linear with respect to the local temperature. This means that a spatial variation in temperature in the sample results in the occurrence of different scattering angles for polychromatic synchrotron radiation. The method of calculation of X-ray diffraction on the basis of local properties is acceptable for a material considered as a mosaic of slightly misoriented single crystals (James, 1950). The method assumes a kinetic approach (incoherent superimposition of scattering intensities). Diffraction in a deformed single crystal can be represented as a reflection on a bent atomic lattice plane (Fig. 1).

Experiments using the geometry of diffraction were carried out at the 'Plasma' scattering station on the eighth beamline of the VEPP-4 synchrotron radiation source at the Budker

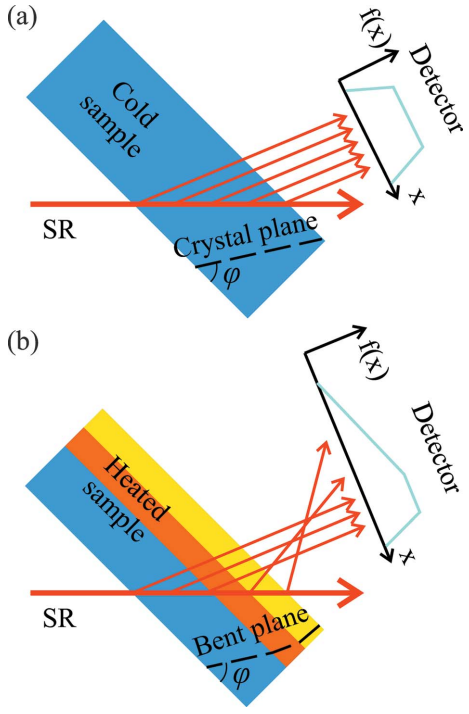

Figure 1
Sketches of the diffraction in a single mosaic crystal exposed to a pulsed heat load. (*a*) Diffraction before heating. (*b*) Diffraction during pulsed heating.

Institute of Nuclear Physics. The scheme of the experiments coincides with that presented by Arakcheev *et al.* (2016). The experiments were performed with polychromatic synchrotron radiation from the wiggler (Vobly *et al.*, 2018). The photon flux from the VEPP-4M storage ring is presented by Zolotarev *et al.* (2016). The distance from the synchrotron radiation source to the sample is close to 40 m.

The chosen sample orientation relative to the beam ensured Laue reflection 110, with the corresponding photon energy below the W *K* edge (69.525 keV) to minimize attenuation in the material. The cross section of the initial beam of synchrotron radiation was 1 mm × 1 mm, so the angular spread of the initial synchrotron radiation was less than 0.002°. The most intense diffraction peak 110 was measured. The scattering angle 2θ corresponding to the energy and diffraction peak was about 4.5°. The choice of 100 single-crystal tungsten was in order to provide the presence of a (110) plane inclined at 45° to the surface and the absence of a preferential direction for plastic deformation along the surface.

We used the one-dimensional detector DIMEX to measure the dynamics of the diffraction peak shape (Arakcheev *et al.*, 2017). The distance from the sample to the detector was about 300 mm. The detector yielded 30 frames containing signals of 512 channels. The width of each channel was 100 µm.

2.2. Pulsed heating

The pulsed heating of the sample was performed by a free-running Nd:YAG laser. The spike regime of the heating does not significantly change the result of the measurements compared with temporally uniform heating because the temperature distribution difference takes place only in a thin surface layer. The duration of the heating pulse was about 140 µs. The 50 J laser radiation was focused to a 5 mm-diameter spot on the sample surface. The heated area was greater than the synchrotron radiation beam cross section (1 mm × 1 mm), so the heating by laser radiation within the synchrotron radiation beam cross section was quite uniform. The emissivity for the 1064 nm wavelength radiation is about 0.4 (De Vos, 1954). The heating parameters make it possible to estimate the surface temperature rise as 2000°C. Thus, according to formula (5), the estimated change in the scattering angle is 1°, but the non-uniformity of the laser-energy release in the heating spot may lead to a substantial inaccuracy in this estimation.

According to expression (5), a change in the diffraction peak shape can be observed only when there is a significant difference between the temperatures of the front and back faces of the sample. The distance of the temperature propagation during pulsed heat load is given by the following formula:

$$L = (\chi\tau)^{1/2}, \tag{6}$$

where L is the typical distance of temperature propagation, χ is the thermal diffusivity and τ is the duration of pulsed heating. The distance L for tungsten under heating for 140 µs is about 200 µm, so the sample thickness was chosen to be equal to 200 µm. Note that this value is close to the attenuation distance for the energy corresponding to the used diffraction peak (below the energy of the W *K*-edge).

Formula (1) assumes heating of a thin surface layer of a thick sample. To bring the heating of a thin sample to the assumed one, we fixed the sample along the perimeter of the heated spot. This prevents the sample from bending and shifting along the surface (Arakcheev, Skovorodin *et al.*, 2015).

3. Results and discussion

We measured the dynamics of the 110 diffraction peak of a 200 µm-thick W(100) single crystal according to the method presented in the previous section. Fig. 2 shows the dynamics of the peak shape, as well as the initial and final states of the peak. The initial state of the peak was measured before the pulsed heating and the final state was measured after a time long enough to reach thermal equilibrium at room temperature. The width of the initial state of the diffraction peak exceeds by far the angular spread of the initial synchrotron radiation, so the latter can be neglected for analysis of the results of the experiments. Three stages in the evolution of the diffraction peak can be clearly distinguished here: heating of the surface, equalization of the temperature distribution normal to the surface (along the depth), and cooling to room temperature.

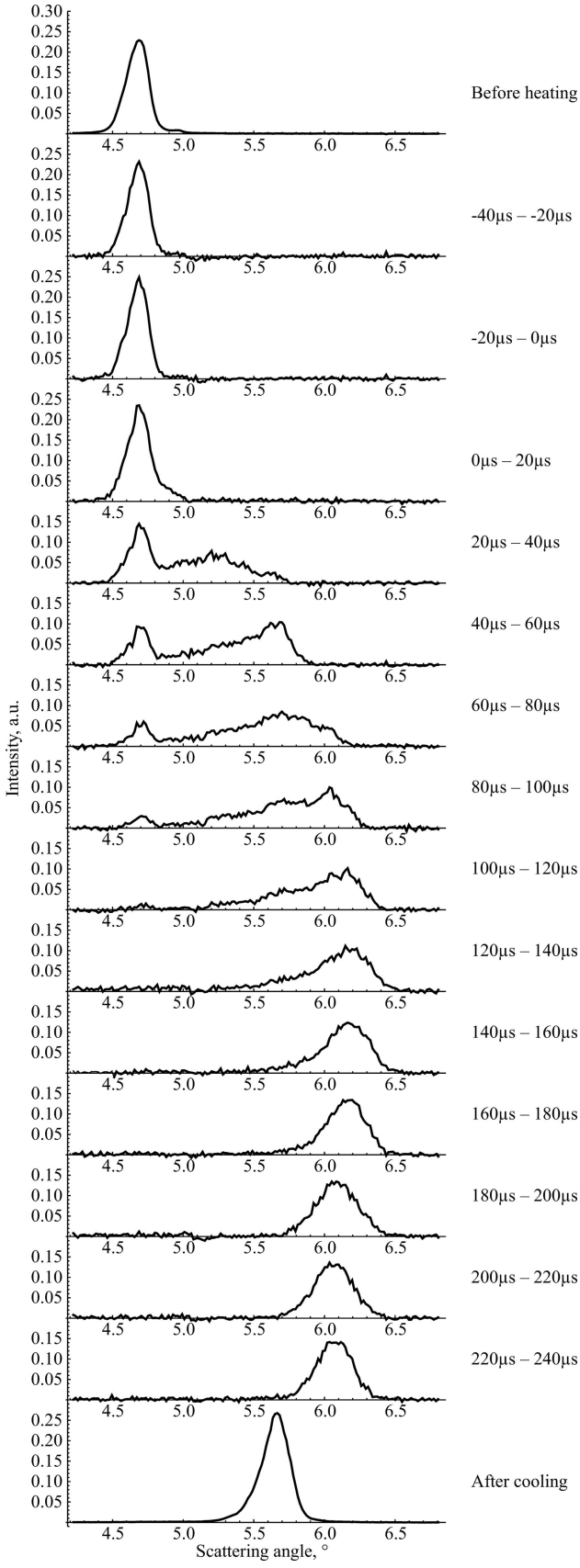

Figure 2
Initial state, final state and dynamics of the 110 diffraction peak of 200 μm-thick 100 single-crystal tungsten during pulsed heat load. The heating started approximately at 0 μs and finished at 140 μs.

3.1. Heating

In the first stage, approximately from 0 to 140 μs (heating by the laser pulse), the surface temperature increases and the thickness of the heated layer grows. The scattering angle of the X-rays grows with temperature in the heated layer according to expression (5). Consequently, part of the initial diffraction peak moves to the right in Fig. 2. At this stage the temperature of the back of the sample stays close to the initial value, which means that layers with all temperatures from the initial one to the instantaneous maximum one are present in the temperature distribution. Therefore, the signal of the scattered radiation covers the whole range from the initial position to the moving right-hand side of the diffraction peak. The deformation distribution is determined by the quite sharp distribution of temperature. As a result, the diffraction peak is complex and non-bell-shaped.

Another feature of this stage is the almost constant position of the initial diffraction peak. The peak position near 4.7° is the result of diffraction by the single crystal at the initial temperature. So, while the thickness of the layer at the initial temperature decreases because of propagation of the heat front, the amplitude of the peak also decreases. The constancy of the peak position confirms the absence of sample bending. Thus, all the changes in the diffraction peak shape are caused by local rotation of the diffraction atomic lattice plane. The observation of the change in shape of the diffraction peak is direct evidence of the predicted effect of atomic lattice-plane rotation induced by local heating because bending of the sample cannot result in the formation of the observed complex shape of the diffraction peak. Qualitatively, a bent sample should just add angular spread of the scattered synchrotron radiation.

Note that the peak of concern at the position of the initial diffraction peak disappears at the end of the first stage, which is an accidental coincidence. Indeed, the heating duration is set by external influences, while the duration of the temperature propagation across the sample depends on the sample material and thickness. The coincidence in this particular case was due to the optimization of the demonstration experiment.

3.2. Equalization of temperature

Equalization of the temperature distribution perpendicular to the surface occurs at the second stage (approximately from 140 to 240 μs). At the beginning of the equalization, the depth distribution of the temperature is non-uniform: the heated side is hot and has an increased scattering angle, whereas the other side has almost the initial temperature and, consequently, the initial value of the scattering angle. Equalization of the temperature means that the colder layers warm up and the hotter layers cool down. Thus, the change in scattering angle is positive at small scattering angles and negative at greater scattering angles. As a result, the diffraction peak becomes narrower (see Fig. 2). However, at the end of this stage, the diffraction peak is wider than the initial peak due to the presence of plastic deformation.

The evolution of the diffraction peak shape slows down significantly after the second stage because further temperature distribution is caused by heat removal around the sample surface. The heat removal around the surface and then to the sample holder is much slower than the equalization of the temperature distribution normal to the surface because the heat has to be transported over a much longer distance. There are no noticeable changes in the diffraction peak shape in the subsequent 14 frames, which are not shown in Fig. 2.

3.3. Cooling

The evolution of the diffraction peak shape during the third stage (cooling to room temperature) was not measured because the cooling requires much more time than the other stages and the detector used was not suitable for long measurements. The final state of the diffraction peak shape was measured several seconds after the end of the heating, when the sample temperature had returned to room temperature. According to the relation between the temperature and the scattering angle, the latter decreases after cooling. However, the diffraction peak did not return to the initial position, implying the formation of residual plastic deformation.

Note that the initial and final states are static, so the diffractograms were measured much more accurately.

3.4. Static measurements

Two more heating pulses were made. The dynamics of the diffraction peak shape were similar to that during the first heating pulse. There was a more remarkable point in the changes in the final diffraction peak shapes and positions after the second and third pulses (Fig. 3). The consistent shift towards larger scattering angles after each pulse means that each pulse leads to an increase in plastic compression along the surface. The dependence of the residual deformation on the depth leads to broadening of the diffraction peak. The increase in the diffraction peak width after each heating pulse is clearly seen in Fig. 3. Evidently, the duration of pulsed heating (~140 μs) is not long enough to attain plastic deformation corresponding to the maximum reached temperature.

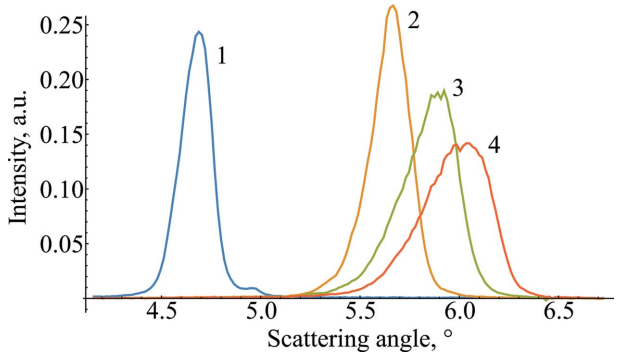

Figure 3
The static 110 diffraction peak before pulsed heating and after each of three heating pulses. (1) Before pulsed heating, (2) after first pulsed heating, (3) after second pulsed heating and (4) after third pulsed heating.

Therefore, the previously used approach of static calculations of plastic deformation (Arakcheev, Huber *et al.*, 2015; Arakcheev, Skovorodin *et al.*, 2015) is not valid for quite short pulsed processes.

4. Summary

Measurements of the dynamics of diffraction peak shape during pulsed heat load were carried out at the 'Plasma' scattering station on the eighth beamline of the VEPP-4 synchrotron radiation source. Changes in the diffraction peak shape were clearly seen. The changes agree qualitatively with the theoretical predictions, and the change in the scattering angle is in agreement with the estimation.

Three stages in the evolution of the diffraction peak can be clearly distinguished: heating, equalization of the temperature, and cooling. The observed change in the diffraction peak shape confirms that the driver is rotation of the atomic lattice plane rather than bending of the material. Moreover, the constancy of the initial diffraction peak position means that the bending is negligible.

Measurements of the diffraction peak before and after several heating pulses have demonstrated that pulsed heating for 140 μs was not long enough to reach the final value of plastic deformation. This should be taken into account for the correct simulation of the pulsed heat load on divertor plates in fusion reactors.

Acknowledgements

This work was supported by program SB RAS V.45.2.3 and was performed using the infrastructure of the Shared-Use Center 'Siberian Synchrotron and Terahertz Radiation Center (SSTRC)' based on VEPP-4M of the BINP, Siberian Branch of the Russian Academy of Sciences.

References

Anderson, C. E. & Brotzen, F. R. (1982). *J. Appl. Phys.* **53**, 292–297.
Arakcheev, A., Ancharov, A. I., Aulchenko, V. M., Bugaev, S. V., Burdakov, A. V., Chernyakin, A. D., Evdokov, O. V., Kasatov, A. A., Kosov, A. V., Piminov, P. A., Polosatkin, S. V., Popov, V. A., Sharafutdinov, M. R., Shekhtman, L. I., Shmakov, A. N., Shoshin, A. A., Skovorodin, D. I., Tolochko, B. P., Vasilyev, A. A., Vyacheslavov, L. N. & Zhulanov, V. V. (2016). *Phys. Procedia*, **84**, 184–188.
Arakcheev, A., Aulchenko, V., Kudashkin, D., Shekhtman, L., Tolochko, B. & Zhulanov, V. (2017). *J. Instrum.* **12**, C06002.
Arakcheev, A., Huber, A., Wirtz, M., Sergienko, G., Steudel, I., Burdakov, A. V., Coenen, J. W., Kreter, A., Linke, J., Mertens, P., Shoshin, A. A., Unterberg, B. & Vasilyev, A. A. (2015). *J. Nucl. Mater.* **463**, 246–249.
Arakcheev, A., Skovorodin, D., Burdakov, A. V., Shoshin, A. A., Polosatkin, S. V., Vasilyev, A. A., Postupaev, V. V., Vyacheslavov, L. N., Kasatov, A. A., Huber, A., Mertens, P., Wirtz, M., Linsmeier, C., Kreter, A., Löwenhoff, T., Begrambekov, L., Grunin, A. & Sadovskiy, Y. (2015). *J. Nucl. Mater.* **467**, 165–171.
De Temmerman, G., Hirai, T. & Pitts, R. A. (2018). *Plasma Phys. Control. Fusion*, **60**, 044018.
De Vos, J. C. (1954). *Physica*, **20**, 690–714.
Hirai, T., Panayotis, S., Barabash, V., Amzallag, C., Escourbiac, F., Durocher, A., Merola, M., Linke, J., Loewenhoff, Th., Pintsuk, G.,

Wirtz, M. & Uytdenhouwen, I. (2016). *Nucl. Mater. Energy*, **9**, 616–622.
Huber, A., Arakcheev, A., Sergienko, G., Steudel, I., Wirtz, M., Burdakov, A. V., Coenen, J. W., Kreter, A., Linke, J., Mertens, P., Philipps, V., Pintsuk, G., Reinhart, M., Samm, U., Shoshin, A., Schweer, B., Unterberg, B. & Zlobinski, M. (2014). *Phys. Scr.* **T159**, 014005.
James, R. W. (1950). *The Optical Principles of the Diffraction of X-rays. The Crystalline State*, Vol. 2. London: Bell and Sons.
Linke, J., Akiba, M., Bolt, H., van der Laan, J., Nickel, H., van Osch, E., Suzuki, S. & Wallura, E. (1992). *J. Nucl. Mater.* **196–198**, 607–611.
Loewenhoff, Th., Linke, J., Pintsuk, G., Pitts, R. A. & Riccardi, B. (2015). *J. Nucl. Mater.* **463**, 202–205.
Makhlaj, V. A., Garkusha, I. E., Malykhin, S. V., Pugachov, A. T., Landman, I., Linke, J., Pestchanyi, S., Chebotarev, V. V. & Tereshin, V. I. (2009). *Phys. Scr.* **T138**, 014060.
Ongena, J., Koch, R., Wolf, R. & Zohm, H. (2016). *Nat. Phys.* **12**, 398–410.
Panayotis, S., Hirai, T., Barabash, V., Durocher, A., Escourbiac, F., Linke, J., Loewenhoff, Th., Merola, M., Pintsuk, G., Uytdenhouwen, I. & Wirtz, M. (2017). *Nucl. Mater. Energy*, **12**, 200–204.
Vobly, P., Baranov, G., Levichev, E., Piminov, P., Zolotarev, K., Havin, N. & Zuev, V. (2018). *IEEE Trans. Appl. Supercond.* **28**, 4101403.
Wagner, F. (2007). *Plasma Phys. Control. Fusion*, **49**, B1–B33.
Zolotarev, K., Kulipanov, G., Levichev, E., Mezentsev, N., Pindyurin, V., Piminov, P. & Tolochko, B. (2016). *Phys. Procedia*, **84**, 4–12.